ELECTRON CLOUD EFFECTS IN ACCELERATORS*

F. Zimmermann†, CERN, Geneva, Switzerland

Abstract

This article presents a brief overview of the electron-cloud problem in charged-particle accelerators. It covers first and historical observations, simulation efforts, past challenges, modelling achievements, recent successes, objectives and future challenges.

PREHISTORY

In 1977, during operation with bunched proton beams at the Intersecting Storage Rings (ISR) a strong pressure rise was experienced in a 7-m long Al chamber in a resonance-like manner at certain combinations of bunch charge and bunch spacing; see Fig. 1. Realizing that an aluminium surface was likely to have a large seconday emission yield, O. Gröbner explained this observation by the new mechanism of "bunch-induced multipactoring" [1].

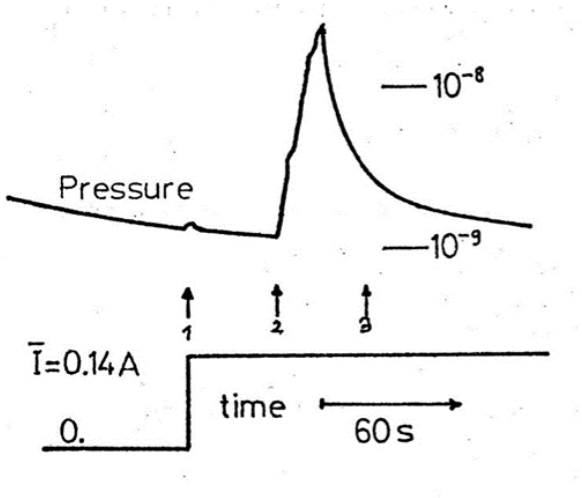

Figure 1: Pressure size observed during slow horizontal displacement of a bunched proton beam across the aperture of an aluminium vacuum chamber at the CERN ISR [1]. The numbered arrows indicate different horizontal beam positions.

In the late 1980, a vertical instability with a peculiar frequency spectrum was seen at the KEK Photon Factory when operated with multi-bunch positron beams. The same type of instability did not occur for electron beams. M. Izawa and co-workers proposed that the positron beam instability was driven by electrons, and applied a simple analytical model, with a wake-field coupling affecting several successive bunches, to explain the frequency spectrum observed [2].

* This work was supported in part by the European Commission under the HORIZON 2020 project ARIES no. 730871.

† frank.zimmermann@cern.ch

Developing the first ever electron-cloud simulation code, PEI, to model the effect of photoelectrons, in the early 1990s, K. Ohmi showed that a simulated multi-bunch instability driven by photoelectrons could indeed explain the observations at the KEK Photon Factory [3]. Figure 2 compares experimental frequency spectra of the positron-beam instability with the analytical model of M. Izawa and with a simulation result from K. Ohmi.

Inspired by K. Ohmi's work, in 1996, M. Furman and G. Lambertson performed electron-cloud simulations for PEP-II, using their new code POSINST, which in addition to the photoelectrons also included the effect of secondary emission [4].

In early 1997, using a separately developed, similar code, ECLOUD, the author performed first electron-cloud simulations for the LHC, revealing a significant electron cloud build up due to both (or either) photo-electrons and secondary electrons [5]. As a result, F. Ruggiero launched a CERN electron-cloud crash program for the LHC [6].

LHC ELECTRON CLOUD

In 1999, the first "LHC beams" stored in the LHC injector, the SPS, experienced electron-cloud driven beam instabilities with different characteristics in the horizontal and vertical plane [7, 8] that could be explained by the electron motion in a vertical magnetic field. From 2000 to 2002, a large number of novel, specialized diagnostics was developed and installed in the SPS [9], such as in situ SEY measurements (for conditioning or "scrubbing" studies) [N. Hilleret], pick-up calorimeters (measuring heat load and energy spectrum) [B. Henrist], strip detectors (spatial distribution) [9], a warm calorimeter (heat) [10] and a cold LHC-prototype vacuum chamber COLDEX [11]. Many of these experimental observations were reviewed in Ref. [9].

As an outcome from these studies and the crash program, an LHC mitigation strategy was defined, consisting of beam screen with (1) sawtooth chamber [13] in proper orientation [14, 15], (2) pumping slot shields [16], and (3) "scrubbing" or the conditioning/decrease of the secondary emission yield as a function of incident electron dose [12, 17–19]. Figure 3 shows the final version of the LHC beam screen; sawtooth and shields are indicated.

The behaviour of the secondary emission yield for low primary electron energies attracted quite some attention, as it greatly affects the survival of secondary electrons before the next bunch arrives. Different models were proposed to describe the low-energy character of the secondary emission yield and fitted to experimental data [12, 18, 19], including data at cryogenic temperature [12].

A few days of "scrubbing" are now routinely scheduled during every LHC start-up. The reconditioning is particularly needed after thermal cycle and venting of a sector. In

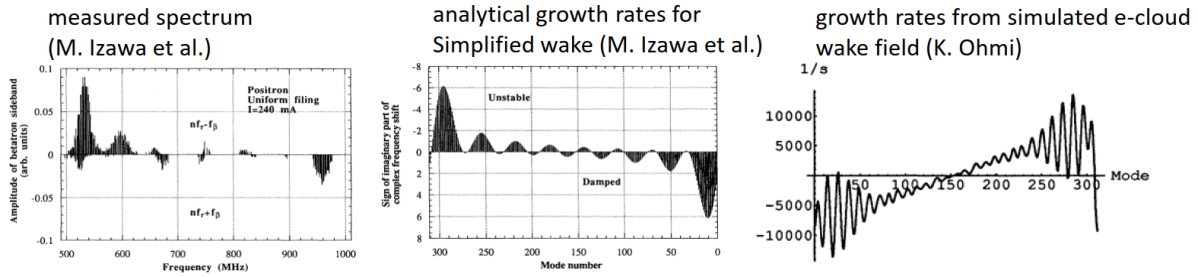

Figure 2: Measured frequency spectrum of unstable positron beam in the KEK Photon Factory [2], growth rates from a simple analytical model with a constant wake field extending over 8 successive bunches [2], and growth rates expected using a more realistic wake field obtained from the simulated photo-electron motion [3].

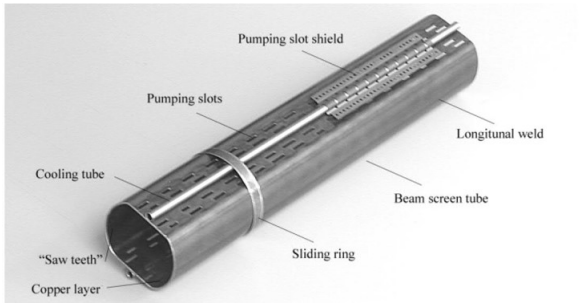

Figure 3: LHC beam screen with sawtooth surface and pumping-slot shields for electron-cloud mitigation [16].

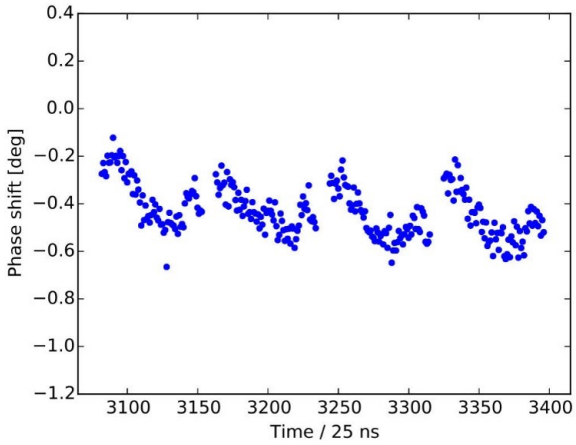

Figure 4: Synchronous phase shift due to electron cloud measured along several bunch trains in the LHC [22].

2017 this reconditioning required about 1 week with standard 25 ns beam. A single day of scrubbing suffices to recondition sectors that were not vented in the preceding shutdown [20, 21].

DIAGNOSTICS

In addition to using pressure rise, heat load and beam instabilities as signals of the electron cloud in the LHC, other diagnostics techniques were also developed. Energy loss of the beam to the electron cloud leads to a synchronous phase shift along a bunch train (see Fig. 4) which can be used to estimate the average electron cloud density around the ring [22]. The energy loss deduced in this way is consistent with the heat load detected by the LHC cryogenics system.

Microwaves can interact with electron clouds in various ways [23, 24]. When electromagnetic waves are transmitted through a not-too-dense electron plasma, they experience a phase shift and possibly a small attenuation. Therefore, another technique to detect the presence of an electron cloud in beam-pipe section of interest relies on an electron-induced modulation of a microwave signal sent through this section [25–29]. This method was tested in the SPS [26], PEP-II [28, 29], the LHC [26], the FNAL Main Injector [30] and the FNAL Recycler [30, 31]. Figure 5 shows an example result from PEP-II, Fig. 6 an example from the FNAL Recycler.

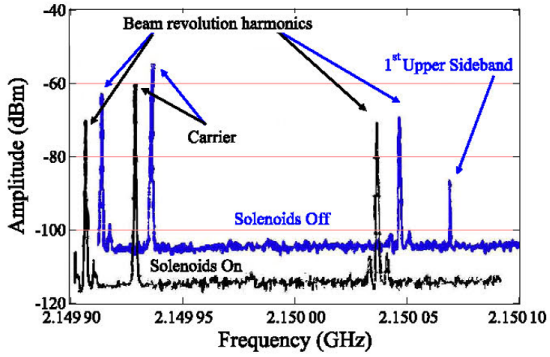

Figure 5: Phase modulated microwave signal at PEP-II [28].

COLLABORATIONS

Collaborations and exchanges with other communities facing similar problems were launched. For example, space satellites with high-power RF systems can be strongly affected by multipacting processes, which depend on the wavelengths and dimensions of the devices in question and on the secondary emission yields. With multifrequency operation the beating field evolution highly resembles the electric field

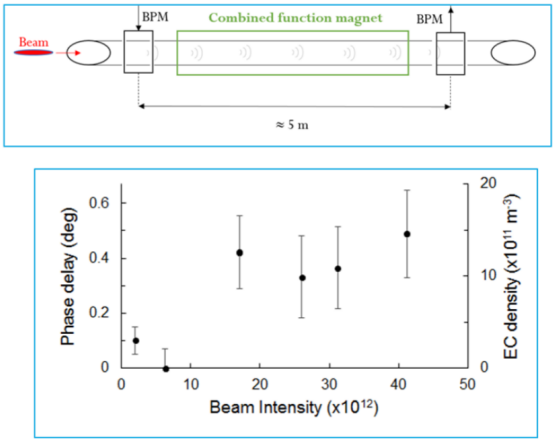

Figure 6: Microwave transmission results at the FNAL Recycler [30, 31].

of successive LHC bunches. The European Space Agency's ESTECH and its partners develop advanced surface coatings and have their own models for the secondary emission yields and its dependence on various parameters. Figure 7 shows F. Caspers and the author during a visit at ESA-ESTECH in Norwijk.

Figure 7: F. Caspers and F. Zimmermann during a 2009 visit at ESA/ESTECH in Norwijk.

ELECTRON-CLOUD DRIVEN INSTABILITY AND EMITTANCE GROWTH

Around 2001/2002, detailed simulation studies revealed that the unstable multi-bunch mode spectrum strongly depends on the magnetic field to which the moving electrons are subjected [32, 33]. At KEKB the installation and activation of weak solenoid fields in the previously field-free regions dramatically altered the mode spectrum of the electron-cloud driven coupled-bunch instability [32, 33].

Simulations and experiments revealed that the electron cloud can be trapped for longer periods of time, not only in the fields of solenoids, but also in the fields of quadrupoles, sextupoles and combined function magnets [31, 34, 35]; see Figs. 8 and 9.

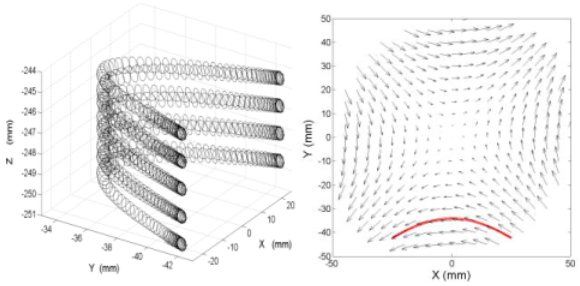

Figure 8: Photoelectron trapping in a magnetic quadrupole field during the bunch train gap at KEKB, simulated by the code CLOUDLAND. Left: 3D orbit; Right: 2D orbit (red line) and quadrupole field (black arrow) [34].

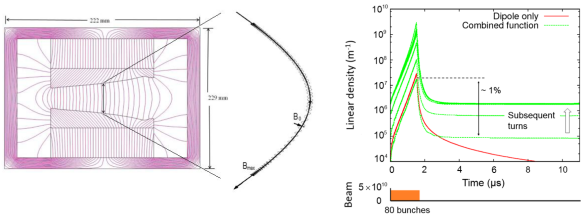

Figure 9: Cross-section of a permanent combined function dipole, at the FNAL Recycler, with indicated trapped electron trajectory (left), and comparison of simulated electron-cloud decay following a bunch-train passage in a pure dipole field and a combined function magnet (right) [31, 35].

At KEKB a strong vertical blow-up was observed above a certain beam current, as is illustrated in Fig. 10. The current threshold value depended on the bunch spacing. The threshold was increased by adding weak solenoid windings in otherwise field-free regions [36]. The synchrotron light diagnostics also indicated a possible residual slow beam size growth below the threshold (Fig. 10).

The fast vertical blow up of the KEKB LER positron beam above the "threshold" could be explained by single-bunch electron-cloud instability, using a 2-particle model [37], simulations [37], and a more refined analytical model based on an approximation through a conventional resonator impedance and interpretation in terms of a TMCI-like instability [38].

For SuperKEKB many countermeasures for electron-cloud suppression were adopted, such as an antechamber for photon capture, TiN coating of the vacuum chamber, grooved surfaces and clearing electrodes inside the wiggler magnets [39]. Figure 11 shows the vertical beam size blow up versus beam current In commissioning phase 1, after the installation of permanent magnets in the uncoated bellows sections. Up to a current of 0.9 A no strong blow up was observed. The design beam current is 3.6 A.

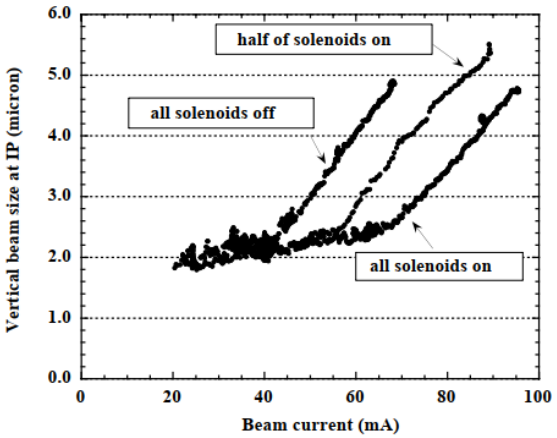

Figure 10: Vertical beam size, measured by the interferometer, versus beam current at the KEKB Low Energy (positron) Ring without and with partial or full solenoid fields in otherwise field-free regions. In the measurement two trains were injected on opposite sides in the ring. Each train contained 60 bunches. The bunch spacing was 4 RF buckets [36].

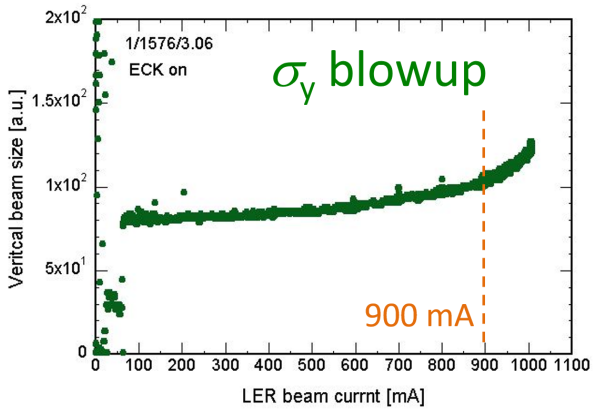

Figure 11: Vertical beam size versus beam current at the SuperKEKB Low Energy (positron) Ring in the commissioning phase 1 after installing permanent magnets at the bellows. In the measurement one long train was injected; the average bunch spacing was 3.06 RF buckets [39, 40].

For proton beams, the electron cloud can drive a similar single-bunch instability. Contrary to conventional instabilities, due to the smaller beam sizes at higher energy and strong electron cloud pinch, at higher proton energies the electron-driven proton beam instability can exhibit a lower threshold, roughly decreasing as $1/\sqrt{\gamma}$. This unfavourable scaling with energy was predicted analytically in 2005 [41, 42], and confirmed three years later in detailed simulations and experiments [43]. Approximating the threshold density as $\rho_{e,\mathrm{thr}} \approx 2\gamma Q_s/(\pi\beta r_p C)/H$ [37], where the pinch enhancement factor H is roughly modelled as increasing in proportion to the number of (small-amplitude) electron oscillations with angular frequency ω_e inside the beam potential, $H \approx 1 + 4\sigma_z\omega_e/(\pi c) \approx 4\sqrt{N_b r_e \sigma_z \gamma/(\sqrt{2\pi}\beta\varepsilon_{\mathrm{N}})}$, the threshold electron density can be estimated as [41, 42]

$$\rho_{e,\mathrm{thr}} \approx \frac{\left(\alpha_c - \frac{1}{\gamma^2}\right)\varepsilon_{||,\mathrm{rms,N}} f_{\mathrm{rf}}}{4\pi^2\sigma_z^2 r_p}\sqrt{\frac{\sqrt{2\pi}\varepsilon_{\mathrm{N}}}{\beta\sigma_z N_b r_e}}\frac{1}{\sqrt{\gamma}} \qquad (1)$$

where f_{rf} denotes the RF frequency, α_c the momentum compaction factor, C the circumference, β the average transverse beta function, σ_z the rms bunch length, N_b the bunch population, r_e the classical electron radius, r_p the classical proton radius, ε_{N} the normalized transverse rms emittance, $\varepsilon_{||,\mathrm{rms,N}}$ the longitudinal normalized rms emittance in units of metre, γ the relativistic Lorentz factor. Eq. (1) assumes $4\sigma_z\omega_e/(\pi c) \gg 1$. The emittances and beta functions of the proton beam were taken to be approximately equal in the horizontal and vertical plane ($\varepsilon_{\mathrm{N}} \approx \varepsilon_{x,\mathrm{N}} \approx \varepsilon_{y,\mathrm{N}}$, $\beta \approx \beta_x \approx \beta_y$).

Figure 12 shows a simulation example [43], which indicates the predicted $1/\sqrt{\gamma}$ behavior [41].

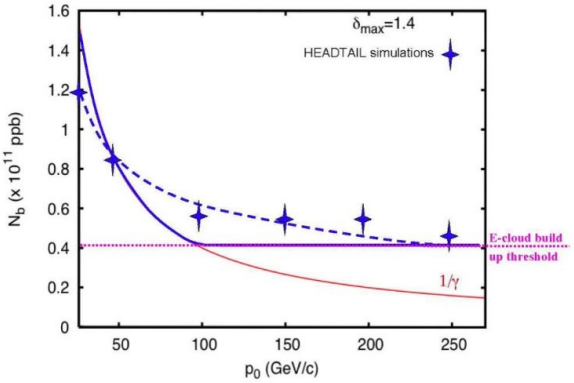

Figure 12: Simulated ECI thresholds at different momenta, study done with quasi-self-consistent e-cloud distribution [43].

If the electron cloud is generated by beam-induced multipacting inside magnets, the electron cloud also shows an unusual dependence on the bunch intensity. At highest proton intensities electrons receive too much energy from a passing bunch, so that the secondary emission yield is no longer maximum, but decreasing with higher incident electron energy. As the bunch intensity decays during a physics store the multipacting region moves closer to the center of the beam pipe, and the central electron-cloud density increases. if the electrons are close to the beam, they can drive a single-bunch instability [37]. Figure 13 shows an example from the LHC [45, 46]. This prediction is consistent with LHC beam observation, where the onset of instability often occurs after a significant decay in the beam intensity.

In addition to coherent beam motion, below the instability threshold the electron cloud can give rise to an incoherent emittance growth [47]. Evidence for such incoherent emittance driven by an electron cloud has been reported from various postron and proton storage rings. At the KEKB B factory already below the instability threshold the measured beam size increased with beam current, though much more

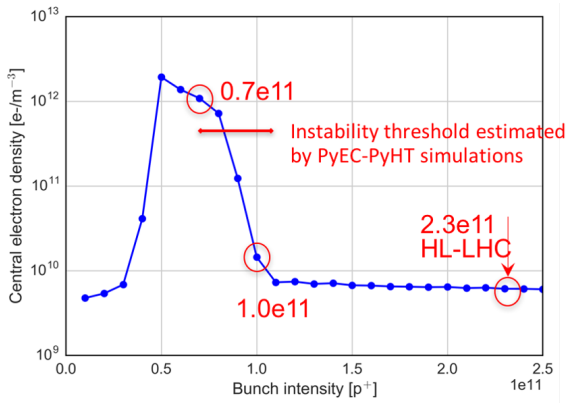

Figure 13: Simulated central electron-cloud density in an LHC dipole magnet as a function of bunch population; also indicated is the expected single-bunch instability threshold (red arrow) obtained from a separate simulation [43].

gradually than above the threshold [36]. Also at RHIC an electron cloud caused emittance growth and beam loss [48]. Similar effects were seen at the Tevatron for 19-ns bunch spacing, without any sign of coherent beam motion [49]. Figure 16 presents the simulated effect of clearing bunches for the FNAL recycler.

MITIGATION METHODS

Proposed techniques of beam manipulations to combat electron cloud build up include the satellites and clearing bunches. Figure 14 shows the concept of satellite bunches for electron-cloud mitigation in the LHC. The simulated effect of satellite bunches for the LHC is illustrated in Fig. 15 [50]. Figure 16 presents similar results for clearing bunches in the FNAL Recycler [35].

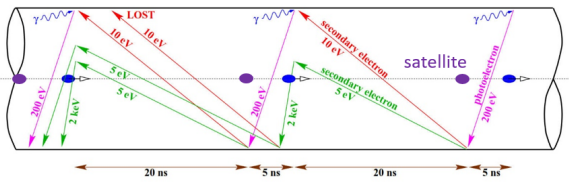

Figure 14: Illustration of intermediate low-intensity satellite bunch deployed for electron-cloud clearing [50] (F. Ruggiero).

A well established standard procedure for electron-cloud suppression is beam scrubbing, that is the operation at the limit of acceptable vacuum pressure or cryogenic heat load for extended periods of time with highest sustainable electron-cloud intensities in order to reduce the secondary emission yield of the vacuum chamber surface, allowing for subsequent safe and electron-free operation at lower beam intensity. Figure 15 illustrates the application of this concept at the LHC, where bunch spacing is a key parameter, determining the strength of the electron cloud. In the LHC, shorter bunch separations lead to enhanced electron-cloud formation, and better surface conditioning. Figure 17 illustrates how, at the LHC "scrubbing" with 25 ns spacing allows for subsequent electron-cloud free operation at 50 ns [51]. Similarly, for fully eliminating electron cloud at a bunch spacing of 25 ns, beam conditioning with a special "doublet" beam — a beam with alternatingly 5 ns and 20 ns spacing — has been considered [51].

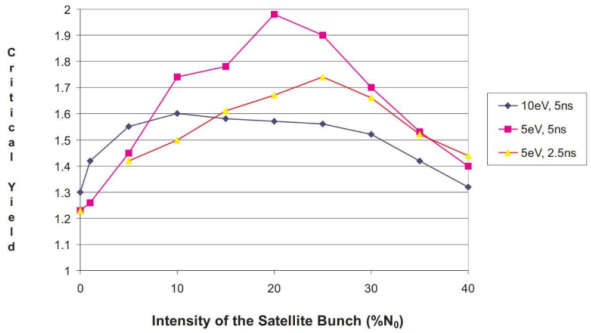

Figure 15: Critical value of the maximum secondary electron yield $\delta_{\max}$ versus the relative intensity of satellite bunches following the nominal bunches at a spacing of 2.5 ns (one LHC RF bucket) or 5 ns (two LHC RF buckets). A highly reflective beam screen surface is assumed, with a surface photon reflectivity $R \simeq 1$, and a half-Gaussian secondary electron energy distribution with 5 eV or 10 eV r.m.s. width [50].

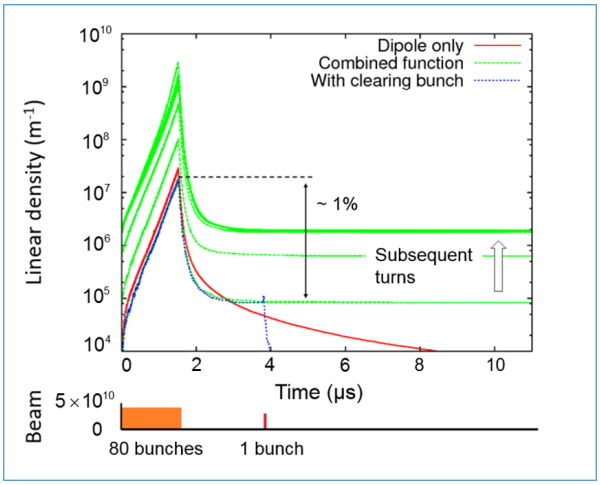

Figure 16: Simulated electron line density in a combined function magnet of the FNAL Recycler as a function of time; a clearing bunch removes the trapped cloud (blue dashed line), preventing the long-term accumulation of electrons [35].

Amorphous carbon (a-C) coating [52] and Laser Ablation Surface Engineering (LASE) [53, 54] of the vacuum chamber surface prior to beam operation are two further, highly efficient schemes for electron-cloud mitigation Both methods dramatically reduce the secondary emission yield. With LASE a maximum secondary emission yield below 1 can be achieved on Cu, Al and stainless steel surfaces;

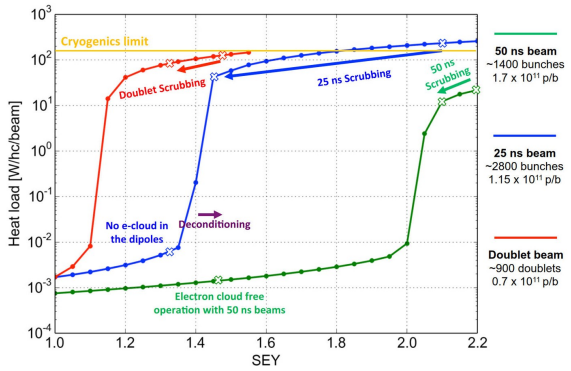

Figure 17: Recipe and effect of LHC beam scrubbing, to prepare for subsequent LHC operation not affected by the electron cloud. The simulated heat load on the LHC dipole beam screen is shown as a function of the SEY for 50 ns (1400 bunches, green line), 25 ns (2800 bunches, blue line) and doublet beams (900 doublets, red line) [51].

see Figs. 18 and 19. The positive effect of LASE has been demonstrated experimentally, with beam in the SPS [55].

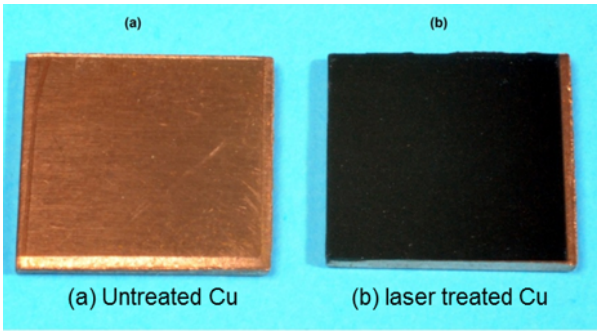

Figure 18: Untreated and laser-treated copper surface [53].

In 2005 an in-situ installation of clearing electrodes was proposed for the LHC [56], as is illustrated in Fig. 20. Presently, another technique for in-situ coating is under development for eRHIC [57, 58]; see Fig. 21. This system could be used to apply various types of coating: Cu, TiN, NEG, and a-C.

MODELLING EFFORTS

Modelling efforts have been discussed and reviewed, among others, at several past two-stream-instability and electron-cloud workshops [59–63]. Figure 22 shows the dream of the CARE-HHH-2004 workshop [64], a complete electron-cloud simulation. We have since come quite a bit closer towards this goal.

Since a few years already, the Warp-Posinst code allows fully self-consistent simulations (many bunches, many turns): of the e-cloud build-up and associated beam dynamics [66]. In particular, Warp-Posinst enabled the first direct simulation of a train of 3×72 LHC-type bunches — using 9,600 CPUs on the Franklin supercomputer (NERSC, U.S.A.). In Fig. 23, we present an example simulation result,

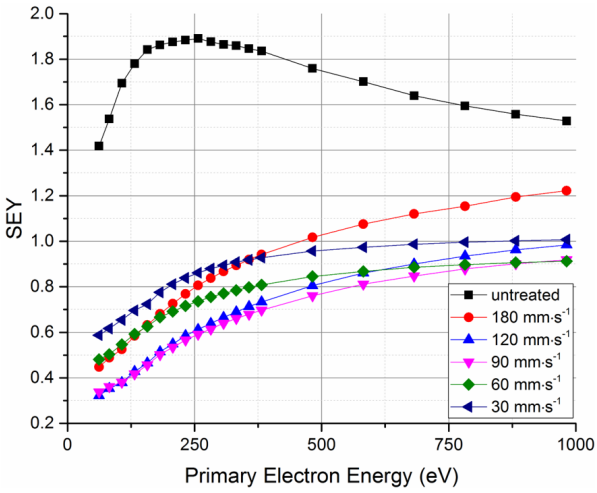

Figure 19: Secondary emission of copper as a function of primary electron energy, without any treatment, and with laser treatment at different processing speeds [54].

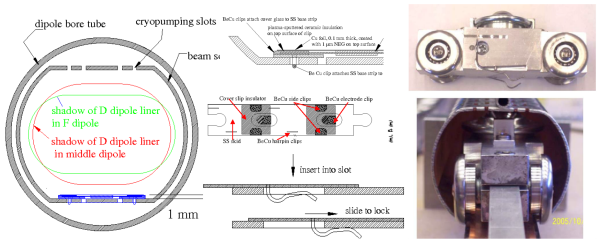

Figure 20: Illustrations of the proposed in-situ installation of LHC clearing electrodes [56].

for the injection of an LHC proton beam into the SPS. A substantial density rise in the tails of the batches is noticeable from turn 0 to turn 800.

LANDAU DAMPING WITH A PINCHING ELECTRON CLOUD

An analytical Landau-damping stability diagram has been constructed for the pinched electron cloud [67]. The model

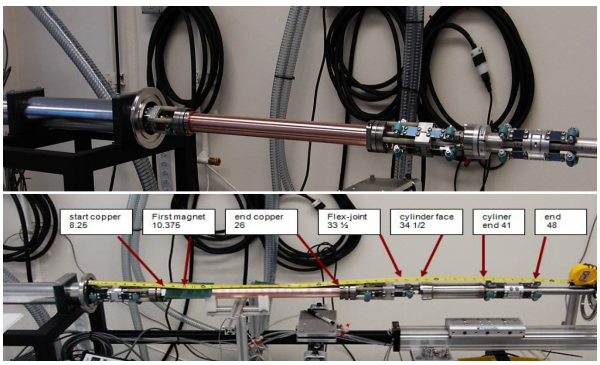

Figure 21: A 50-cm long cathode magnetron mole assembly for in-situ coating of the RHIC vacuum chamber [57, 58].

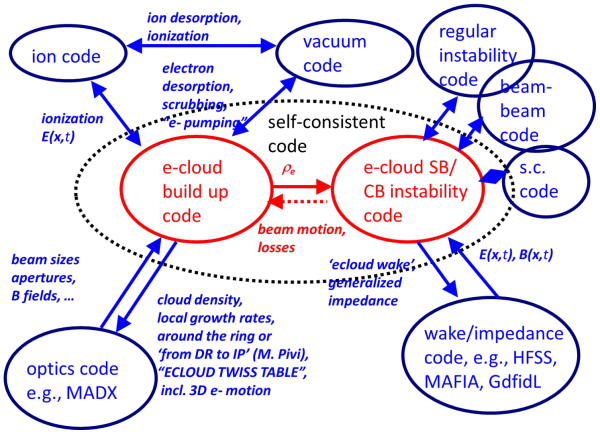

Figure 22: Schematic of the 'ultimate' electron-cloud code sketched in 2004 [65].

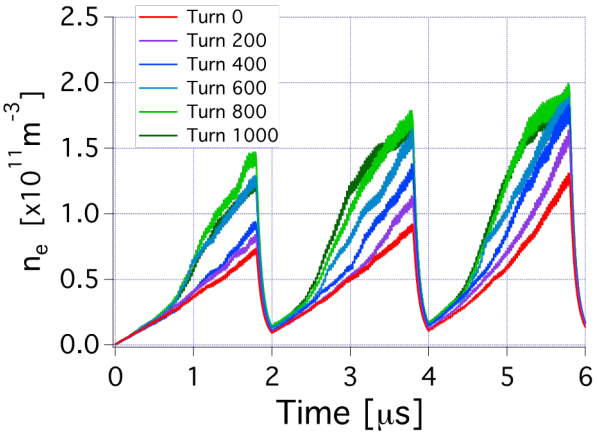

Figure 23: Average electron cloud density history seen at a fixed station [66].

assumes a quasi-parabolic profile (Fig. 24 left)

$$\rho_b(z) = \frac{15}{16\sqrt{7}\sigma_z}\left(1-\frac{y^2}{7\sigma_z^2}\right)^2 , \qquad (2)$$

and a linear tune shift along the bunch, as a first order approximation of the effect of the electron-cloud pinch,

$$\Delta Q_{ec}(z) = \frac{z-\sqrt{7}\sigma_z}{\sqrt{7}\sigma_z}\Delta Q_{ec,max} ; \qquad (3)$$

see the right picture of Fig. 24. The latter can be converted to

$$z = \frac{\sqrt{7}(2\Delta Q_{ec}+\Delta Q_{ec,max})\sigma_z}{\Delta Q_{ec,max}} . \qquad (4)$$

Together with (2), this yields

$$\rho_b(\Delta Q_{ec}) = \frac{15}{8\Delta Q_{ec,max}}\left(1-\left(\frac{2\Delta Q_{ec}-\Delta Q_{ec,max}}{\Delta Q_{ec,max}}\right)^2\right)^2 . \qquad (5)$$

Combining formalisms and recipes from H.G. Hereward [68], D. Möhl and H. Schönauer [69], A.E. Chao [70],

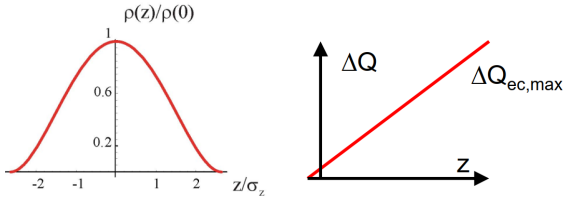

Figure 24: Bunch profile (left) and approximate tune shift along the bunch due to the pinching electron cloud (right), as assumed in the analytical Landau damping model [67].

J.S. Berg [71], E. Métral and F. Ruggiero [72], and assuming a synchrotron period is long compared with the instability rise time leads to the dispersion relation

$$\begin{aligned} 1 &= -\int_0^{\Delta Q_{ec,max}} dQ_{ec}\,\frac{\rho(\Delta Q_{ec})\,[\Delta Q_{coh}-\Delta Q_{ec}]}{Q_0+\Delta Q_{ec}-Q} \\ &= -\Big[P.V.\int_0^{\Delta Q_{ec,max}} dQ_{ec}\,\frac{\rho(\Delta Q_{ec})\,[\Delta Q_{coh}-\Delta Q_{ec}]}{Q_0+\Delta Q_{ec}-Q} \\ &\quad +i\pi\rho(Q-Q_0)\,[\Delta Q_{coh}-Q+Q_0]\Big] , \end{aligned} \qquad (6)$$

which can be rewritten as

$$\Delta Q_{coh} = -\frac{P.V.\int_0^{\Delta Q_{ec,max}} dQ_{ec}\,\frac{\rho(\Delta Q_{ec})\Delta Q_{ec}}{\Delta Q_{ec}-\Delta Q}+i\pi\rho(\Delta Q)\Delta Q-1}{P.V.\int_0^{\Delta Q_{ec,max}} dQ_{ec}\,\frac{\rho(\Delta Q_{ec})}{\Delta Q_{ec}-\Delta Q}+i\pi\rho(\Delta Q)} . \qquad (7)$$

where $\Delta Q \equiv Q - Q_0$ is the net physical tune shift, and ΔQ_{coh} is the coherent tune shift due to an external machine impedance. We can now plot the trace when ΔQ runs along the real axes (border of stability) in the complex ΔQ_{coh} plane. The result is displayed in Fig. 25. Though the electron potential moves with the beam, the electron cloud alone creates non-trivial stability diagram. We note that $\Delta Q_{ec,max}$ can be huge, of order 0.1–0.2.

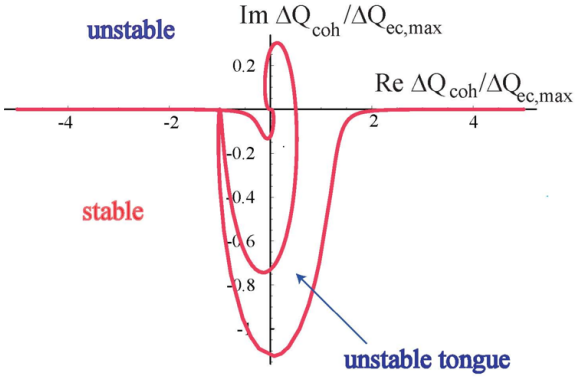

Figure 25: Stability diagram in the presence of a pinching electron cloud [67].

16L2

An interesting effect was seen at the LHC in 2017/18. Apparently limited to a short region "16L2" of the LHC ring,

this phenomenon was marked by loss spikes and fast beam instabilities. The 16L2 problem was mitigated by introducing groups of empty buckets inside the bunch trains and by locally adding weak magnets fields, both cures characteristic of an "electron cloud". The 16L2 was finally explained by a local electron cloud (plus, possibly, an accompanying ion cloud) of high density. The local electron-cloud activity was later attributed to a frozen layer of air and/or water on the surface extending over a few meters length, which had been caused by an accidental air inlet through an adjacent pumping port; see Fig. 26.

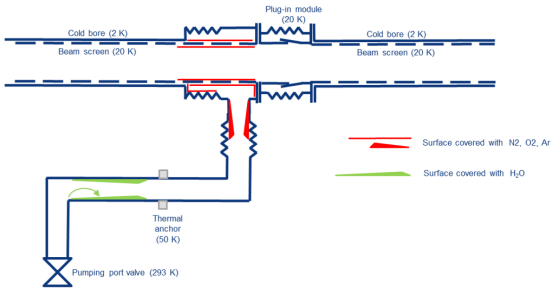

Figure 26: A frozen layer of water and/or air at the LHC's 16L2 location [73].

ELECTRON CLOUD IN THE FCC

Electron cloud is a concern for the proton rings of the proposed 100 TeV hadron collider, FCC-hh [74], with much enhanced synchrotron radiation compared with the LHC, and also for the positron ring of the future circular electron-positron collider, FCC-ee [75]. The FCC hadron-collider beam screen and the lepton-collider vacuum system are illustrated in Fig. 27. Different types of antechambers and advanced surface treatments like LASE, for FCC-hh, and a novel (ultrathin) NEG coating developed for FCC-ee [76,77], will help suppress electron-cloud buildup without a noticeable increase in the machine impedance.

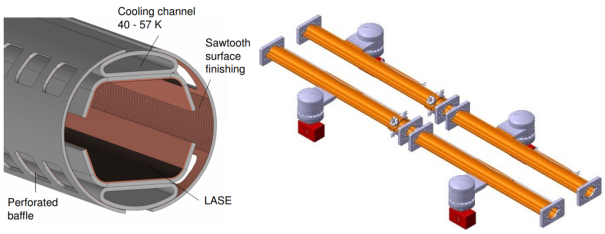

Figure 27: Beam screen for the FCC-hh arcs, with a "folded" integrated antechamber and LASE surface treatment [74] (left), and FCC-ee vacuum chambers with an antechamber, discrete local photon stops, adjacent or opposite pumping domes, and ultra0thin NEG coating [75] (right). Vacuum-chamber optimisation for both FCC-hh hand FCC-ee took into account the need for electron-cloud suppression.

The superiority of the new FCC-hh beam screen design compared with the LHC beam screen is apparent from a comparison of the respective simulated heat load and central electron-density for the HE-LHC [78] (an LHC energy doubler based on FCC-hh magnet technology); see Fig. 28.

The modelling for FCC-ee brings forth new challenges, e.g., related to the energy of the synchrotron-radiation photons. At FCC-ee, photo-electrons are generated via classical photo-effects, but additional, energetic electrons are emitted after an atomic de-excitation [79, 80]. The threshold value for the second process is about 1 keV; for comparison the critical photon energy in the FCC-ee arcs at the $t\bar{t}$ threshold is of order 1 MeV. The atomic deexcitation phenomenon has been integrated with the photon tracking code, SYNRAD3D [81].

Finally, it is interesting to note that the electron cloud itself may interact with the propagating synchrotron radiation [82]. If such effect proved important, this would require yet another level of self-consistency in the electron-cloud modelling effort, where photons and electrons are so far treated fully independently.

FROM LHC TO HL-LHC

The arc heat loads have already been a challenge for LHC Run 2 (2015–2018) with 25 ns bunch spacing, where the LHC operated close to cryogenics limits in some of the arcs. In these arcs the heat load was much larger than expected from impedance and synchrotron radiation. A large differences was observed between sectors; see Fig. 29. A corresponding difference in the electron-cloud behavior between sectors is (or was) the most plausible explanation. The extrapolated HL-LHC heat loads for the high-load sectors would not be acceptable [83, 84].

The highest heat has been found in the sectors around the ATLAS experiment. There has been much speculation as to what was different in the high-load sectors, causing the difference in heat load. Possible explanations included shielding from cosmic rays by the Jura mountains, the changes which may have occurred during the installation/production sequence, or the effect of an inverted, missing or differently shaped sawtooth surface on the beam screen (Fig. 30).

EPILOGUE

In January 2018, the Chair of the LHC Machine Advisory Committee stressed that "LHC electron cloud is a top priority for the LHC and for CERN!" [88]. The same statement, of course, applies to any other future accelerator operating with positively charged particle beams.

ACKNOWLEDGEMENTS

I would like to thank G. Arduini, E. Belli, M. Benedikt, R. Cimino, G. Franchetti, M. Giovannozzi, G. Iadarola, K. Oide, L. Mether, E. Métral, M. Migliorati, G. Rumolo, D. Schulte, and M. Vretenar for helpful discussions and continuous encouragement.

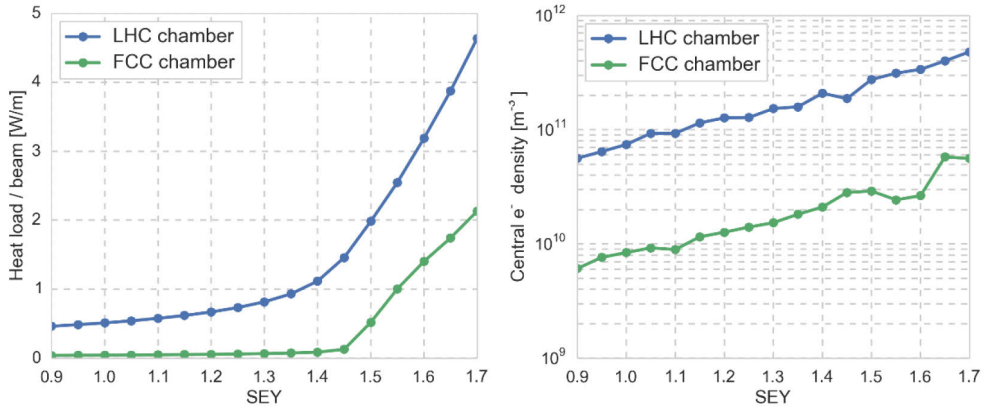

Figure 28: Simulated heat load (left) and central electron density (right) for the HE-LHC [78], comparing an LHC-type beam screen (blue) and the beamscreen designed for FCC-hh (green) (L. Mether).

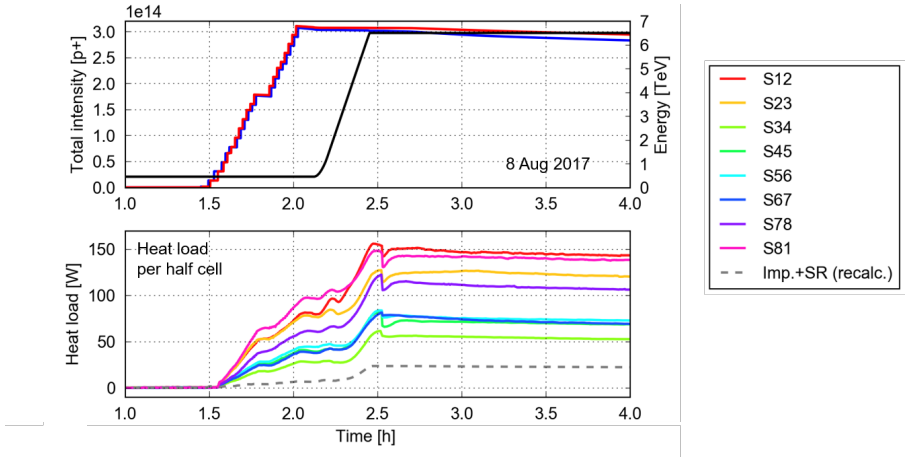

Figure 29: Total beam intensity (top) and heat load per half cell in each of the 8 LHC sectors (bottom) during 4 hours in 2017 [83, 84].

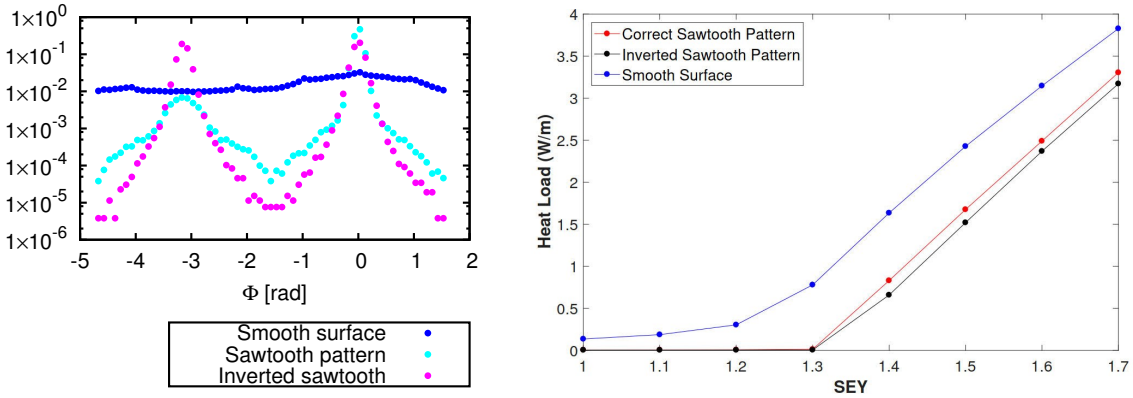

Figure 30: Azimuthal distribution of absorbed synchrotron-radiation photons [85] simulated with the code SYNRAD3D (left) and heat load per metre as a function of the maximum secondary emission yield for different sawtooth configurations [86] simulated by using the SYNRAD3D results as input for the code PyECLOUD [87] (right).

REFERENCES

[1] O. Gröbner,"Bunch Induced Multipactoring", presented at the International Conference on High Energy Accelerators, Serpukhov 1977, CERN-ISR-VA 77-38 (1977).

[2] M. Izawa, Y. Sato, and T. Toyomasu, "The Vertical Instabiity in a Positron Bunched Beam," Phys. Rev. Lett. 74, 25 (1995) 5044.

[3] K. Ohmi, "Beam-Photoelectron Interactions in Positron Storage Rings," Phys. Rev. Lett. 75, 8 (1995) 1526.

[4] M.A. Furman and G.R. Lambertson, "The Electron-Cloud Instability in PEP-II," Proc. EPAC'96 Sitges, LBNL 38220 (1996).

[5] F. Zimmermann, "A simulation study of electron-cloud instability and beam-induced multipacting in the LHC," CERN LHC-Project-Report-95, SLAC-PUB-7425 (1997).

[6] LHC Electron Cloud Crash Programme, web site `http://ab-abp-rlc.web.cern.ch/ab-abp-rlc-ecloud/`

[7] G. Arduini et al., "Transverse Instabilities of the LHC Proton Beam in the SPS," Proc. 7th European Particle Accelerator Conference, Vienna, Austria (2000) 341.

[8] K. Cornelis, "The Electron Cloud Instability in the SPS," Proc. Mini Workshop on Electron Cloud Simulations for Proton and Positron Beams, CERN, Geneva, Switzerland, 15–18 April 2002, CERN-2002-001 (2002) pp. 11–16.

[9] J.M. Jimenez et al., "Electron Cloud with LHC-Type Beams in the SPS: A Review of Three Years of Measurements,âĂİ LHC Project Report 632 (2002).

[10] V. Baglin, B. Jenninger, "SPS electron cloud heat load measurements with WAMPAC and simulations," Proc. ini Workshop on Electron Cloud Simulations for Proton and Positron Beams, CERN, Geneva, Switzerland, 15–18 April 2002, CERN-2002-001 (2002) pp. 79–85.

[11] V. Baglin, I.R. Collins, B. Jenninger, "Performance of a Cryogenic Vacuum System (COLDEX) with a LHC Type Proton Beam," CERN-LHC-Project-Report-667

[12] R. Cimino, I.R. Collins et al., "Can Low-Energy Electrons Affect High-Energy Physics Accelerators?," Phys. Rev.'Lett.'93, 014801 (2004).

[13] I. Collins, "Electron cloud investigations," CERN SL Seminar, Thursday 11 November 1999 (1999) `https://indico.cern.ch/event/413583`.

[14] N. Kos, Engineering Change Order - Class I "Change of Beam screen Types in CryoDipoles for Sector 3-4," LHC-VSS-EC-0010 ver. 1.0, EDMS Document no. 985318, June 2009.

[15] G. Guillermo, D. Sagan, and F. Zimmermann, "Examining mitigation schemes for synchrotron radiation in high-energy hadron colliders," Phys. Rev. Accel. Beams 21, 021001 (2018).

[16] O.S. Brüning et al., "LHC Design Report vol. 1", CERN Yellow Report CERN-2004-003-V-1, Section 12.3.1. (2004).

[17] O.S. Brüning et al., "Electron Cloud and Beam Scrubbing in the LHC," Proc. 18th Biennial Particle Accelerator Conference, New York, NY, USA, 29 March – 2 April 1999 (1999) 2629. and CERN LHC-Project-Report-290

[18] V. Baglin et al., "A Summary of Main Experimental Results Concerning the Secondary Electron Emission of Copper," CERN LHC-Project-Report-472 (2001).

[19] R.E. Kirby, F.K. King, "Secondary electron emission yields from PEP-II accelerator materials," Nucl. Instr. Meth. A 469 (2001) 1–12.

[20] G. Iadarola, L. Mether, G. Rumolo, "Filling schemes and e-cloud constraints for 2017," Proc. 7th Evian Workshop on LHC beam operation, Evian Les Bains, France, 13–15 Dec. 2016 (2016) pp. 239–244.

[21] M. Solfaroli, "Machine configuration and parameters," 8th LHC Operations Evian Workshop, Evian, 12–14 December 2017 `https://indico.cern.ch/event/663598/`.

[22] J. F. Esteban Müller, P. Baudrenghien, T. Mastoridis, E. Shaposhnikova, and D. Valuch, "High-accuracy diagnostic tool for electron cloud observation in the LHC based on synchronous phase measurements," Phys. Rev. ST Accel. Beams 18, 112801 (2015)

[23] F.J. Decker, F. Caspers, F. Zimmermann, "Impact of Microwaves on the Electron Cloud and Incoherent Effects," Proc. Mini Workshop on Electron Cloud Simulations for Proton and Positron Beams, CERN, Geneva, Switzerland, 15–18 April 2002 (2002) pp. 87–90.

[24] M. Mattes, E. Sorolla, F. Zimmermann, arXiv:1310.0212 Proc. Joint INFN-CERN-EuCARD-AccNet Workshop on Electron-Cloud Effects: ECLOUD'12; 5–9 June 2012, La Biodola, Isola d'Elba, Italy, CERN-2013-002 (2012) pp. 177–180.

[25] F. Caspers, F. Zimmermann, "Interactions of Microwaves and Electron Clouds," Proc. Particle Accelerator Conference 2009, Vancouver, Canada, 04–08 May 2009 (2009) pp. WE1PBI02

[26] T. Kroyer et al., "Unexpected results on microwave waveguide mode transmission measurements in the SPS beam pipe," in Proc. 31st Advanced ICFA Beam Dynamics Workshop on Electron-Cloud Effects, Napa, CA, USA, 19–23 April 2004 (2004) pp. 89–94

[27] T. Kroyer, F. Caspers, E. Mahner, "The CERN-SPS Experiment on Microwave Transmission through the Beam Pipe," Proc. 21st IEEE Particle Accelerator Conference, Knoxville, TN, USA, 16–20 May 2005 (2005) pp. 2212

[28] M. T. F. Pivi et al., "Microwave Transmission Measurement of the Electron Cloud Density in the Positron Ring of PEP-II," in Proc. 11th European Particle Accelerator Conference, Genoa, Italy, 23 - 27 Jun 2008 (2008) pp. MOPP065

[29] S. De Santis et al., "Measurement of Electron Clouds in Large Accelerators by Microwave Dispersion," Phys. Rev. Lett. 100 (2008) 094801

[30] J. S. Eldred et al., "Electron Cloud Measurements in Fermilab Main Injector and Recycler," Proc. IPAC2015 (2015) MOPMA027

[31] S. A. Antipov, "Fast Transverse Beam Instability Caused by Electron Cloud Trapped in Combined Function Magnets," Springer Theses (2018) ISBN 3030024083, 9783030024086

[32] S. S. Win, H. Fukuma, S. Kurokawa, K. Ohmi, "Study Of Coupled Bunch Instability Caused By Electron Cloud In Kekb Positron Ring," Proc. 8th European Particle Accelerator Conference, Paris, France, 3–7 June 2002 (2002) pp. 1592

[33] S. S. Win et al., "Numerical study of coupled-bunch instability caused by an electron cloud," Phys. Rev. ST Accel. Beams 8, 094401 (2005).

[34] L. Wang, H. Fukuma, S. Kurokawa, K. Ohmi, K. Oide, "Photoelectron Trapping in Electric and Magetic Field," in Proc. 8th European Particle Accelerator Conference, Paris, France, 3–7 June 2002 (2002) pp. 1586.

[35] S. A. Antipov, S. Nagaitsev, "Electron Cloud Trapping In Recycler Combined Function Dipole Magnets," PoS ICHEP2016 (2017) 773, doi: 10.22323/1.282.0773.

[36] H. Fukuma, "Electron Cloud Effects at KEKB," Proc. Mini Workshop on Electron Cloud Simulations for Proton and Positron Beams, CERN, Geneva, Switzerland, 15–18 April 2002, CERN-2002-001 (2002) pp. 1–9; doi: 10.5170/CERN-2002-001.1

[37] K. Ohmi, F. Zimmermann, "Head-tail instability caused by electron cloud in positron storage rings," Phys. Rev. Lett. 85 (2000) 3821–3824.

[38] K. Ohmi, F. Zimmermann, E. A. Perevedentsev, "Wake-field and fast head-tail instability caused by an electron cloud," Phys. Rev. E 65 (2001) 016502.

[39] Y. Suetsugu et al., "Mitigating the electron cloud effect in the SuperKEKB positron ring," Phys. Rev. Accel. Beams 22, 023201 (2019).

[40] Y. Suetsugu, "Updates of SKEKB MR Vacuum System," 22nd KEKB Review, 14 Match 2018.

[41] F. Zimmermann, "Scaling the Electron Cloud Instability Threshold to Higher SPS Energy," presented at CERN ABP-RLC Meeting, 18 Nov. 2005 http://ab-abp-rlc.web.cern.ch/ab-abp-rlc/Meetings/2005/2005.11.18/ScalingWithEnergy-FZ.pdf

[42] F. Zimmermann, "Overview of Electron-Cloud Effects in the LHC and Present Understanding," CERN-GSI bi-lateral working meeting on Collective EffectsâĂŞCoordination of Theory and Experiments, 30 March 2006 http://care-hhh.web.cern.ch/care-hhh/Collective\%20Effects-GSI-March-2006/default.html

[43] G. Rumolo, G. Arduini, E. Métral, E. Shaposhnikova, E. Benedetto, R. Calaga, G. Papotti, and B. Salvant, "Dependence of the Electron-Cloud Instability on the Beam Energy," Phys. Rev. Lett. 100, 144801 (2008).

[44] O. Domínguez, K. Li, G. Arduini, E. Métral, G. Rumolo, F. Zimmermann, and H. Maury Cuna, "First electron-cloud studies at the Large Hadron Collider," Phys. Rev. ST Accel.'Beams 16, 011003 (2013).

[45] A. Romano et al., "Electron cloud buildup driving spontaneous vertical instabilities of stored beams in the Large Hadron Collider," Phys. Rev. Accel. Beams 21, 061002 (2018).

[46] R. D'Agnolo et al, "Strategy for Extreme Beam Facilities," CERN-ACC-2017-0033, ARIES Monograph XLIV, Institute of Electronic Systems, Warsaw University of Technology, Warsaw, 2017, edited by F. Zimmermann (2017).

[47] E. Benedetto, G. Franchetti, F. Zimmermann, "Incoherent effects of electron cloud in proton storage rings," Phys. Rev. Lett. 97 (2006) 034801.

[48] J. Wei et al., "Observation of Electron-Ion Effects at RHIC Transition," in Proc. 2005 Particle Accelerator Conference (PAC), Knoxville, Tennessee, 2005, edited by C. Horak (2005) p. 4087.

[49] Xiaolong Zhang, email to Francesco Ruggiero, October 2005

[50] Francesco Ruggiero and Xiaolong Zhang, "Collective Instabilities in the LHC: Electron Cloud and Satellite Bunches," in Proc. Workshop on Instabilities of High Intensity Hadron Beams in Rings, Upton, NY, USA, 28 June – 1 July 1999, edited by T. Roser and S.Y. Zhang, Amer. Inst. Phys., AIP Conference Proceedings 496 (1999) pp. 40–48.

[51] G. Iadarola, G. Rumolo, "Electron Cloud and Scrubbing: Perspective and Requirements for 25 ns Operation in 2015," in Proc. 5th Evian Workshop on LHC beam operation, Evian-les-Bains, France, 2–4 June 2014, CERN-ACC-2014-0319 (2014) pp. 81–92.

[52] C. Yin Vallgren et al., "Amorphous Carbon Coatings for Mitigation of Electron Cloud in the CERN SPS," in Proc. 1st International Particle Accelerator Conference, Kyoto, Japan, 23–28 May 2010 (2010) pp. TUPD048

[53] O Malyshev, "Laser Ablation Surface Engineered (LASE) surfaces for e-cloud mitigation," FCC-hh impedance and beam screen workshop, CERN, 30–31 March 2017 (2017).

[54] R. Valizadeh et al., "Reduction of secondary electron yield for E-cloud mitigation by laser ablation surface engineering," Applied Surface Science, Vol. 404, 15 (2017) 370–379 doi: 10.1016/j.apsusc.2017.02.013.

[55] S. Calatroni et al., "First accelerator test of vacuum components with laser-engineered surfaces for electron-cloud mitigation," Phys. Rev. Accel. Beams 20 (2017) 113201

[56] P. M. McIntyre, A. Sattarov, "illing the Electron Cloud Effect in the LHC Arcs," Proc. 21st IEEE Particle Accelerator Conference, Knoxville, TN, USA, 16–20 May 2005 (2005) pp. 2971

[57] A. Hershcovitch et al., "Recent RHIC in-situ coating technology developments," Proc. Joint INFN-CERN-EuCARD-AccNet Workshop on Electron-Cloud Effects, La Biodola, Isola d'Elba, Italy, 5–9 Jun 2012, CERN-2013-002 (2013) pp. 251–258

[58] A. Hershcovitch et al., "Device and Technique for In-situ Coating of the RHIC Cold Bore Vacuum Tubes with Thick OFHC," Proc. 4th International Particle Accelerator Conference, Shanghai, China, 12–17 May 2013 (2013) pp. 3508

[59] Workshop on Two-Stream Instabilities - Two-Stream Instabilities, KEK, Tsukuba, Japan, 11—14 September 2001; http://conference.kek.jp/two-stream/.

[60] Mini Workshop on Electron Cloud Simulations for Proton and Positron Beams — ECLOUD'02, CERN, 15 –18 April 2002. Proc. edited by G. Rumolo and F. Zimmermann, CERN-2002-001 (2002).

[61] 31st Advanced ICFA Beam Dynamics Workshop on Electron-Cloud Effects — ECLOUD'04, Napa, CA, USA, 19–23 April 2004. Proc. edited by M. Furman, S. Henderson, and F. Zimmermann, CERN-2005-001 (2005).

[62] International Workshop on Electron-Cloud Effects — ECLOUD'07, Daegu, Korea, April 9–12, 2007. Proc. edited by H. Fukuma, K. Ohmi, and E.-S. Kim, KEK Proceedings 2007-10 (2007).

[63] Joint INFN-CERN-EuCARD-AccNet Workshop on Electron-Cloud Effects — ECLOUD'12, La Biodola, Isola d'Elba, Italy. Proc. edited by R. Cimino, G. Rumolo, and F. Zimmermann, CERN-2013-002 (2013).

[64] 1st CARE-HHH-APD Workshop on Beam Dynamics in Future Hadron Colliders and Rapidly Cycling High-Intensity Synchrotrons — "HHH 2004", CERN, Geneva, Switzerland, 8–11 November 2004. Proc. edited by F. Ruggiero, W. Scandale, and F. Zimmermann, CERN-2005-006 (2005).

[65] F. Zimmermann, "Summary of Panel Discussion on Electron-Cloud Simulation Codes", in Proc. HHH-2004 [64] (2005) p. 297

[66] M.A. Furman, J.-L. Vay, M. Venturini, "Direct Numerical Modeling of E-Cloud Driven Instability of Three Consecutive Batches in the CERN SPS," Proc. IPAC 2012, New Orleans, USA (2012) 1125-1127

[67] F. Zimmermann, "Stability Diagram with Electron Cloud," presented at CERN ABP-RLC Meeting, 7 July 2006 http://ab-abp-rlc.web.cern.ch/ab-abp-rlc/Meetings/2006/2006.07.07/stability\%20diagram\%20with\%20e-cloud.ppt

[68] H. G. Hereward, "Landau damping by non-linearity," CERN-MPS-DL-69-11 (1969).

[69] D. Möhl and H. Schönauer, "Landau damping by non-linear space-charge forces and octupoles," in Proc. 9th International Conference on High-energy Accelerators, SLAC, Stanford, CA, USA, 2–7 May 1974 (1974) pp. 380–384

[70] A. W. Chao, Physics of collective beam instabilities in high energy accelerators, published by Wiley, New York, USA (1993).

[71] J. Scott Berg and F. Ruggiero, "Landau Damping with two-dimensional betatron tune spread", CERN SL-AP-96-71 (AP) (1996).

[72] E. Métral and F. Ruggiero, "Landau damping with two-dimensional betatron tune spread from both octupoles and non-linear space charge," in Proc. 9th European Particle Accelerator Conference, Lucerne, Switzerland, 5–9 July 2004 (2004) pp. 1897

[73] F. Bordry, "LHC Performance Workshop (Chamonix'18) Summary," CERN, 7 March 2018.

[74] M. Benedikt et al., "FCC-hh: The Hadron Collider", The European Physical Journal Special Topics 228, 4 (2019) 755–1107; 10.1140/epjst/e2019-900087-0

[75] M. Benedikt et al., "FCC-ee: The Lepton Collider", The European Physical Journal Special Topics 228, 2 (2019) 261–623; 10.1140/epjst/e2019-900045-4

[76] E. Belli et al., "Electron cloud buildup and impedance effects on beam dynamics in the Future Circular e+e- Collider and experimental characterization of thin TiZrV vacuum chamber coatings," Phys. Rev. Accel. Beams 21 (2018) 111002

[77] E. Belli, "Coupling Impedance and Single Beam Collective Effects for the Future Circular Collider (Lepton Option)," PhD Thesis Sapienza, CERN-THESIS-2018-381 (2018).

[78] F. Zimmermann et al., "HE-LHC: The High-Energy Large Hadron Collider", The European Physical Journal Special Topics 228, 5 (2019) 1109–1382; 10.1140/epjst/e2019-900088-6

[79] S. Poprocki, J. A. Crittenden, D. L. Rubin, D. Sagan, "Modeling Studies for Synchrotron-Radiation-Induced Electron Producyion in the Vacuum Chamber Walls at CesrTA," Proc. 9th International Particle Accelerator Conference IPAC2018, Vancouver, BC, Canada (2018) 3011.

[80] S. Poprocki et al., "Measurement and modeling of electron-cloud-induced betatron tune shifts at the Cornell Electron-Positron Storage Ring test accelerator," Phys. Rev. Accel. Beams 22, 081001 (2019).

[81] G. Dugan and D. Sagan, "Simulating synchrotron radiation in accelerators including diffuse and specular reflections," Phys. Rev. Accel. Beams 20, 020708 (2017).

[82] D. I. Kaltchev and F. Zimmermann, "On the Transparency of the Electron Cloud to Synchrotron Radiation," Proc. Mini Workshop on Electron Cloud Simulations for Proton and Positron Beams, CERN, Geneva, Switzerland, 15–18 April 2002, CERN-2002-001 (2002) pp. 243–250.

[83] G. Iadarola, "Digesting the LIU high brightness beam: is this an issue for HL-LHC?", Chamonix'18 LHC Performance Workshop (2018).

[84] L. Tavian,' "Report from the task force on beam induced heat load", Chamonix'18 LHC Performance Workshop (2018).

[85] G. Guillermo, D. Sagan, and F. Zimmermann, "Examining mitigation schemes for synchrotron radiation in high-energy hadron colliders," Phys. Rev. Accel. Beams 21, 021001 (2018).

[86] G. Guillermo Canton, G.H.I. Maury Cuna, E. Ocampo, F. Zimmermann, "Electron Cloud Build Up for LHC Sawtooth Vacuum Chamber," in Proc. 9th International Particle Accelerator Conference, Vancouver, Canada, 29 April – 4 May 2018 (2018) TUPAF030

[87] G. Iadarola, E. Belli, K. Li, L. Mether, A. Romano, and G. Rumolo, "Evolution of Python Tools for the Simulation of Electron Cloud Effects," CERN-ACC-2017-240 (2017).

[88] N. Holtkamp, private communication, 18 January 2018.